



**HAL**  
open science

## Quantitative nanoscopy of inhibitory synapses: counting gephyrin molecules and receptor binding sites

Christian G. Specht, Ignacio Izeddin, Pamela C. Rodriguez, Mohamed El Beheiry, Philippe Rostaing, Xavier Darzacq, Maxime Dahan, Antoine Triller

### ► To cite this version:

Christian G. Specht, Ignacio Izeddin, Pamela C. Rodriguez, Mohamed El Beheiry, Philippe Rostaing, et al.. Quantitative nanoscopy of inhibitory synapses: counting gephyrin molecules and receptor binding sites. *Neuron*, 2013, 79 (2), pp.308-321. 10.1016/j.neuron.2013.05.013 . hal-04343663

**HAL Id: hal-04343663**

**<https://hal.science/hal-04343663v1>**

Submitted on 13 Dec 2023

**HAL** is a multi-disciplinary open access archive for the deposit and dissemination of scientific research documents, whether they are published or not. The documents may come from teaching and research institutions in France or abroad, or from public or private research centers.

L'archive ouverte pluridisciplinaire **HAL**, est destinée au dépôt et à la diffusion de documents scientifiques de niveau recherche, publiés ou non, émanant des établissements d'enseignement et de recherche français ou étrangers, des laboratoires publics ou privés.

# **Quantitative nanoscopy of inhibitory synapses: counting gephyrin molecules and receptor binding sites**

Christian G. Specht <sup>1,5</sup>, Ignacio Izeddin <sup>2,4,5</sup>, Pamela C. Rodriguez <sup>1</sup>, Mohamed El Beheiry <sup>2,3</sup>,  
Philippe Rostaing <sup>1</sup>, Xavier Darzacq <sup>4</sup>, Maxime Dahan <sup>2,3</sup> and Antoine Triller <sup>1,\*</sup>

<sup>1</sup> Biologie Cellulaire de la Synapse, Inserm U1024, Institute of Biology, École Normale Supérieure (ENS), 46 rue d'Ulm, 75005 Paris, France

<sup>2</sup> Laboratoire Kastler Brossel, CNRS UMR 8552, Department of Physics and Institute of Biology, ENS, Université Pierre et Marie Curie-Paris6, 46 rue d'Ulm, 75005 Paris, France

<sup>3</sup> Present address: Physico-Chimie Curie, Institut Curie, CNRS UMR 168, Université Pierre et Marie Curie-Paris6, 26 rue d'Ulm, 75005 Paris, France

<sup>4</sup> Functional Imaging of Transcription, CNRS UMR 8197, Institute of Biology, ENS, 46 rue d'Ulm, 75005 Paris, France

<sup>5</sup> CGS and II contributed equally to this work.

\*Correspondence: [triller@biologie.ens.fr](mailto:triller@biologie.ens.fr)

## Summary

The strength of synaptic transmission is controlled by the number and activity of neurotransmitter receptors. Yet, little is known about absolute numbers and densities of receptor and scaffold proteins and the stoichiometry of molecular interactions at synapses. Here, we conducted three-dimensional and quantitative nanoscopic imaging based on single molecule detections to characterise the ultra-structure of inhibitory synapses and to count scaffold proteins and receptor binding sites. We observed a close correspondence between the spatial organisation of gephyrin scaffolds and glycine receptors at spinal cord synapses. Endogenous gephyrin was clustered at densities of 5000-10000 molecules per  $\mu\text{m}^2$ . The stoichiometry between gephyrin molecules and receptor binding sites was approximately 1:1, consistent with a two-dimensional scaffold in which all gephyrin molecules can contribute to receptor binding. The competition of glycine and GABA<sub>A</sub> receptor complexes for synaptic binding sites highlights the potential of single molecule imaging to quantify synaptic plasticity on the nanoscopic scale.

## Introduction

The molecular architecture of synapses determines the synaptic strength at a given steady state. Modular scaffold proteins are decisive factors for the internal organisation of synapses. They provide binding sites for the transient immobilisation of neurotransmitter receptors in the postsynaptic membrane, thus setting the gain on synaptic transmission. In addition, synaptic scaffold proteins bind to cytoskeletal elements and regulate downstream signalling events in the postsynaptic density (PSD). In view of this it is essential to know the actual numbers of scaffold proteins to assess their roles for the ultra-structure, function and plasticity of synapses in quantitative terms. Here, we have developed nanoscopic techniques based on single molecule imaging that enable us to gain quantitative insights into the molecular organisation of inhibitory synapses in spinal cord neurons.

The PSDs of inhibitory synapses are characterised by dense clusters of the scaffold protein gephyrin that offer binding sites for inhibitory glycine receptors (GlyRs) and GABA<sub>A</sub> receptors (GABA<sub>A</sub>Rs). The formation and maintenance of these clusters depend on receptor-gephyrin and gephyrin-gephyrin interactions (Calamai et al., 2009). Gephyrin molecules have the capacity to trimerise and to dimerise at their N-terminal (G) and C-terminal (E) domains, respectively (Schwarz et al., 2001;

Sola et al., 2001; Xiang et al., 2001; Sola et al., 2004). These properties have given rise to a model whereby gephyrin forms a hexagonal lattice underneath the synaptic membrane (Kneussel and Betz, 2000; Xiang et al., 2001; Sola et al., 2004), with common binding sites for GlyR $\beta$  and the GABA<sub>A</sub>R subunits  $\alpha$ 1-3,  $\beta$ 2 and  $\beta$ 3 (Maric et al., 2011; Kowalczyk et al., 2013). Electron microscopy (EM) has confirmed that inhibitory PSDs are indeed flat discs with a surface of 0.04-0.15  $\mu\text{m}^2$  and a thickness of  $\sim$ 33 nm, and that gephyrin molecules are clustered at a relatively constant distance from the synaptic membrane (Carlin et al., 1980; Triller et al., 1985; Triller et al., 1986; Nusser et al., 1997; Nusser et al., 1998; Kasugai et al., 2010; Lushnikova et al., 2011).

Despite the overall stability of synaptic structures, inhibitory PSDs are highly dynamic molecular assemblies that can assume simple (macular) or more complex (perforated or segmented) shapes (Lushnikova et al., 2011). Gephyrin molecules exchange continuously between synaptic and non-synaptic populations (Calamai et al., 2009), while synaptic gephyrin clusters may merge or split into separate structures (Dobie and Craig, 2011; Lushnikova et al., 2011). It is believed that the clustering of gephyrin is regulated by posttranslational modifications. A recent study has argued convincingly that alternative splicing and phosphorylation of the central (C) domain of gephyrin plays a crucial role in the folding, receptor-binding and oligomerisation of gephyrin (Herweg and Schwarz, 2012). For example, proline-directed phosphorylation of the gephyrin C domain at residues S188, S194 and/or S200 has been shown to trigger Pin1-dependent conformational changes that augment GlyR binding (Zita et al., 2007). Also, it has been shown that the clustering properties of gephyrin are regulated by protein phosphatase 1 activity and by GSK3 $\beta$  and CDK-dependent phosphorylation of residue S270 (Bausen et al., 2010; Tyagarajan et al., 2011; Kuhse et al., 2012; Tyagarajan et al., 2013).

Various upstream mechanisms such as integrin signalling, collybistin-binding, and excitatory synaptic activity can affect gephyrin clustering (Bannai et al., 2009; Charrier et al., 2010; Papadopoulos and Soykan, 2011). In hippocampal neurons, the induction of synaptic plasticity at excitatory synapses has been shown to increase the size and complexity of inhibitory PSDs (Nusser et al., 1998; Bourne and Harris, 2011; Lushnikova et al., 2011). The morphological plasticity of inhibitory synapses is directly related to the accumulation of inhibitory receptors, as judged by the close correspondence between the size of the PSD and both GABAergic and glycinergic synaptic currents (Nusser et al., 1997; Lim et al., 1999; Kasugai et al., 2010). The number of endogenous

GABA<sub>A</sub>R complexes at synapses has been estimated to vary from 30 to as many as 200 (Nusser et al., 1997 and references cited therein) and that of GlyRs from 10 to 70 (Singer and Berger, 1999; Rigo et al., 2003). Yet, nothing is known about the absolute numbers of gephyrin molecules at inhibitory synapses and about the relative stoichiometry of receptors and scaffold proteins. Here, we make use of quantitative, dynamic, and three-dimensional nanoscopic imaging not only to determine the sub-synaptic distribution of gephyrin and receptor complexes at inhibitory PSDs, but also to count the number of gephyrin molecules and receptor binding sites.

## Results

### Photoactivated localisation microscopy of synaptic gephyrin clusters

With this project our goal was to visualise inhibitory synapses at super-resolution and to extract detailed structural and quantitative information about the postsynaptic density (PSD). We carried out photoactivated localisation microscopy (PALM) on rat dissociated spinal cord cultured neurons expressing photoconvertible constructs of the synaptic scaffold protein gephyrin (mEos2- or Dendra2-gephyrin). PALM was first done on fixed neurons as described in the methods section. The positions of single fluorophores were determined by Gaussian fitting of their point-spread function (PSF) and were corrected for lateral drifts using fiducial markers. The localisation accuracy was estimated as the standard deviation  $\sigma$  of multiple detections of the same fluorophore in subsequent image frames (Izeddin et al., 2011). The precision of localisation was marginally better for mEos2-gephyrin ( $\sigma_x = 11.2 \pm 1.9$  nm mean  $\pm$  SD,  $\sigma_y = 11.9 \pm 1.4$  nm,  $n = 12$  fluorophores) than for Dendra2-gephyrin ( $\sigma_x = 13.1 \pm 2.1$  nm,  $\sigma_y = 12.8 \pm 2.0$  nm,  $n = 11$ ).

When expressed in spinal cord neurons, mEos2-gephyrin and Dendra2-gephyrin accumulate in dense clusters that are visible by conventional fluorescence microscopy (Fig. 1A). PALM imaging makes it possible to measure the sizes of these structures with high precision (spatial resolution  $\sim 25$ - $30$  nm). Image segmentation of the rendered PALM images indicates an apparent surface ranging from  $0.01$  to  $0.1 \mu\text{m}^2$  (Fig. 1B). The PALM experiments also revealed the presence of an additional population of gephyrin clusters below  $0.01 \mu\text{m}^2$  that is not visible in the diffraction-limited images (Fig. 1A,B). To determine the subcellular localisation of both types of clusters we combined PALM imaging with direct stochastic optical reconstruction microscopy (dSTORM) as described previously (Izeddin et al., 2011). In these experiments, the presynaptic protein bassoon

was labelled with Alexa 647-tagged antibodies. Dual-colour PALM/STORM images show the apposition of the large gephyrin clusters with bassoon-positive structures, identifying them as inhibitory PSDs (Fig. 1C). In contrast, gephyrin nanoclusters did not co-localise with bassoon and thus represent a non-synaptic population of gephyrin.

#### The internal organisation of synaptic gephyrin clusters

Upon closer inspection, synaptic gephyrin clusters do not appear to have a uniform shape. As judged by PALM, gephyrin clusters are frequently elongated or twisted in one way or another and may be composed of sub-domains with varying fluorophore densities (Fig. 2A). To rule out the possibility that the presence of sub-domains of gephyrin results from an inadequate sampling of the synaptic scaffold due to the stochastic nature of PALM, we constructed pointillist images from temporally separated sets of movie frames. The similar overall shape and distribution of the fluorophore detections in these images corroborates the heterogeneous distribution of mEos2-gephyrin at inhibitory synapses in fixed spinal cord neurons. Still, chemical fixation could also induce a redistribution of gephyrin and the formation of sub-synaptic protein aggregates. We therefore acquired live PALM movies of about 7 min at 50 Hz from spinal cord neurons expressing mEos2-gephyrin (Fig. 2B). To exclude that lateral movements of the gephyrin clusters (Hanus et al., 2006; Dobie and Craig, 2011) create false representations of their shape, the fluorophore positions in each frame were readjusted to the centre of mass of a given cluster. In other words, the structure itself served as a fiducial marker, and a sliding window of 2000 frames was chosen to align its position over time. As in fixed neurons, gephyrin clusters were often composed of sub-domains with different fluorophore densities. These gephyrin domains changed their relative position on a time scale of minutes. Dynamic PALM imaging thus provides a means to visualise the morphing of the synaptic scaffold.

In order to relate the ultra-structures of synaptic gephyrin clusters to the sub-synaptic distribution of inhibitory neurotransmitter receptors, we did dual PALM/STORM experiments with endogenous GlyRs (Fig. 2C). As expected, GlyR $\alpha$ 1 labelling co-localised extensively with mEos2-gephyrin clusters, due to the direct interaction between gephyrin and the intracellular domain of the  $\beta$  subunit ( $\beta$ -loop) of the receptor complex (Fritschy et al., 2008). In fact, the GlyRs matched the sub-synaptic distribution of gephyrin closely, including the localisation in sub-domains of gephyrin. The co-localisation of GlyR complexes with gephyrin nanoclusters (< 50 nm distance) was also observed

occasionally (Fig. 2C), in agreement with the known interaction between the two proteins outside of synapses (Ehrensperger et al., 2007).

To probe the GlyR-gephyrin interaction at synapses in living neurons, we combined PALM imaging with single particle tracking (SPT) of endogenous GlyR complexes using quantum dots (QD). Dynamic imaging of mEos2-gephyrin and GlyR $\alpha$ 1 coupled with QDs emitting at 705 nm was done simultaneously using a dual-view system. As before, the fluorophore positions in both channels were corrected for the x/y-displacement of the centre of mass of the mEos2-gephyrin cluster. In this way, the trajectories of receptor complexes could be related to the internal morphology of the gephyrin cluster (Fig. 2D). Endogenous GlyRs generally co-localised with gephyrin clusters and were confined within sub-domains of the PSD. Synaptic GlyR complexes displayed a restricted movement, changing their position within gephyrin clusters on a time scale of tens of seconds. This exchange of GlyRs between sub-domains of the gephyrin cluster is seen as a shift in the distribution of individual QD detections, likely representing receptor binding at spatially separated binding sites. Taken together, our observations show that gephyrin clusters have an intricate internal organisation and that their ultra-structure determines the sub-synaptic distribution and diffusion properties of GlyRs.

### The three-dimensional organisation of inhibitory synapses

In the previous experiments, the organisation of inhibitory PSDs was deduced from 2D image projections, which could influence the apparent distribution of synaptic components. We therefore implemented 3D nanoscopic imaging using adaptive optics (Izeddin et al., 2012) to resolve the spatial organisation of inhibitory synapses in spinal cord neurons. This technique makes use of a deformable mirror in the imaging path to optimise the signal detection and, by way of an astigmatic deformation, to retrieve 3D information about the position of single fluorophores below the diffraction limit (Huang et al., 2008).

Dual-colour 3D-PALM/STORM experiments were carried out on mEos2-gephyrin clusters and Alexa 647-tagged GlyR $\alpha$ 1 complexes in fixed spinal cord neurons. As in the 2D experiments, the distribution of GlyRs closely matched the internal organisation of the gephyrin clusters. However, rotation of the 3D images showed that scaffold proteins and receptor domains were shifted relative to one another (Fig. 3A). We determined the distance between the gephyrin molecules and the

receptors along an axis across the PSD, by measuring the distribution of fluorophore detections within a 200 nm radius (Fig. 3B). The mean distance between the labelled GlyRs and mEos2-gephyrin was  $44 \pm 6$  nm (mean  $\pm$  SEM,  $n = 26$  clusters). The GlyR profile itself was in average  $135 \pm 20$  nm wide, and that of gephyrin  $140 \pm 11$  nm (FWHM of fluorophore detections,  $n = 10$  cluster profiles). Since the surface labelling of GlyRs can be considered as essentially two-dimensional, the distribution of the Alexa 647 fluorophores reflects the limit of resolution of our imaging conditions (z-axis pointing accuracy  $\sigma_z = 20$ -30 nm, Izeddin et al., 2012). In addition, we rendered the surfaces of gephyrin and GlyR clusters in order to calculate the volumes of the two domains (Fig. 3C, movie S1). The mean volume of the GlyR domain was  $0.010 \pm 0.006 \mu\text{m}^3$  and that of the gephyrin clusters was  $0.012 \pm 0.006 \mu\text{m}^3$  (mean  $\pm$  SD,  $n = 26$  clusters, 5 fields of view, 3 experiments), although these values may well be an overestimate given the limit of spatial resolution imposed by 3D-PALM. However, this analysis confirmed that the apparent volumes occupied by GlyRs and gephyrin scaffolds were linearly correlated with a slope of 0.8.

#### Quantification of gephyrin molecules in fixed neurons

The strength of synaptic transmission is directly related to the number and activity of neurotransmitter receptors at synapses. Receptor numbers in turn depend on the number of available receptor binding sites. We therefore devised strategies for the quantification of densely packed synaptic proteins in fixed spinal cord neurons. Our first approach was based on the sequential photoconversion of clustered Dendra2-gephyrin molecules and the counting of their photobleaching steps. This was validated with another, independent strategy of molecule counting, consisting in the bleaching of non-converted Dendra2-gephyrin clusters and the calibration of their total fluorescence with the mean fluorescence intensity of single fluorophores. The advantage of the second approach is that it does not require photoconvertible probes, meaning that it can be used for the quantification of conventional fluorophores (see below).

Making use of the photoconversion of Dendra2-gephyrin, we first applied 100 ms pulses of 405 nm to convert small subsets of fluorophores, which were bleached by continuous illumination with a 561 nm laser (Fig. 4A1). The pool of non-converted Dendra2 was depleted by the end of these recordings. Dendra2 was chosen because it is less prone to blinking than mEos2 (Annibale et al., 2011). Importantly, the decay traces exhibited steps of fluorescence intensity associated with single converted (red) Dendra2 (Fig. 4A2). The peak intensities of the pulses could thus be translated into



numbers of fluorophores. The sum of all the peak intensities then yielded the total number of Dendra2-gephyrin molecules within the cluster. This value was related to the fluorescence intensity of the non-converted (green) Dendra2-gephyrin image taken with the mercury lamp prior to the recording, to obtain a conversion factor  $\varphi$  of fluorescence intensity per molecule ( $\varphi = 92 \pm 12$  arbitrary units of fluorescence / molecule, mean  $\pm$  SEM,  $n = 14$  clusters from 9 fields of view and 3 independent experiments). This conversion was then used to quantify a large set of fluorescence images, which suggested that synaptic clusters contain between tens and several hundred Dendra2-gephyrin molecules, with an average of  $218 \pm 9$  (mean  $\pm$  SEM,  $n = 622$  clusters from 42 cells and 3 experiments; Fig. 4A3).

As an alternative approach to quantify the number of gephyrin molecules at inhibitory synapses, we determined the single molecule intensity and the lifetime of the non-converted (green) Dendra2 fluorophores. First, synaptic Dendra2-gephyrin clusters were fully bleached with 491 nm laser illumination (Fig. 4B1). The bleaching traces were fitted with a double exponential decay, which provided the total cluster fluorescence  $A$  (the area under the curve), as well as the weighted time constant  $\tau_w$  of the fluorophore fluorescence lifetime. In order to determine the average intensity  $I$  of single Dendra2 fluorophores, we measured individual blinking events at the end of the acquired movies (Fig. 4B2). Using these parameters, the number of clustered Dendra2-gephyrin molecules was calculated (see methods). As described above, this number was applied to the green fluorescence image taken with the lamp previously, and extrapolated to a larger set of Dendra2-gephyrin clusters, yielding an average of  $211 \pm 9$  molecules per cluster ( $n = 622$  clusters, 42 cells, 3 experiments; Fig. 4B3). Notably, the conversion factor ( $\varphi = 95 \pm 9$  a.u. / molecule,  $n = 48$  clusters, 12 fields of view, 3 experiments) was almost the same as that obtained with the first quantification method. As a result, the two types of quantification, that of the converted and of the non-converted populations of Dendra2-gephyrin gave almost identical results.

#### Numbers and densities of endogenous gephyrin molecules at synapses

Since the quantification of fluorophores through decay recording and single fluorophore detection did not require the use of photoconvertible probes, we used the same approach to quantify the number of endogenous gephyrin molecules in spinal cord neurons from a knock-in (KI) mouse strain expressing mRFP-gephyrin (Calamai et al., 2009). Synaptic clusters of mRFP-gephyrin in fixed dissociated cultures were imaged with a mercury lamp (Fig. 5A), then bleached with 561 nm

laser illumination to measure the total fluorescence of the clusters as well as the time constant and intensity of mRFP fluorophores. The calculated conversion factor  $\varphi$  was applied to other fluorescence images of mRFP-gephyrin clusters, which revealed that synaptic clusters contain between 40 and 500 endogenous gephyrin molecules with an average of  $194 \pm 5$  molecules (mean  $\pm$  SEM,  $n = 829$  clusters from 41 cells and 5 experiments). A similar distribution was found in live recordings (Fig. 5B; mean  $154 \pm 3$  molecules,  $n = 850$  clusters, 41 cells, 3 experiments), indicating that chemical fixation did not have a drastic effect on gephyrin clustering. Interestingly, the absolute numbers of endogenous mRFP-gephyrin molecules at synapses were similar to those of recombinant Dendra2-gephyrin (Fig. 4 & 5B). This suggests that the number of gephyrin molecules at synapses is kept relatively constant, regardless of the protein expression levels. To test this hypothesis, we transfected mRFP-gephyrin KI cultures with Dendra2-gephyrin and sequentially quantified the endogenous and recombinant fluorophores in fixed neurons (bleaching of mRFP at 561 nm followed by Dendra2 at 491 nm). These experiments showed that recombinant Dendra2-gephyrin indeed displaces endogenous mRFP-gephyrin in a dose-dependent manner. Moreover, the combined mRFP- plus Dendra2-gephyrin numbers were remarkably independent of Dendra2-gephyrin overexpression, confirming that the synaptic clustering of gephyrin is tightly regulated in spinal cord neurons (Fig. S1).

To estimate the endogenous mRFP-gephyrin numbers at synapses *in vivo*, we conducted decay recordings on fixed spinal cords from 3 month-old KI animals. The tissue was frozen and sliced in sucrose to preserve the mRFP fluorescence (Fig. 5A). Unexpectedly, the numbers of clustered gephyrin molecules in spinal cord slices were much higher than in cultured neurons (mean  $477 \pm 16$  molecules,  $n = 666$  clusters from 6 spinal cord slices; Fig. 5B). This disparity could be attributed either to the size of the gephyrin clusters or to the density of clustered molecules. In order to distinguish between these possibilities, we reconstructed PALM-like images from the detections of blinking mRFP fluorophores at the end of the photobleaching recordings (referred to as non-activated PALM or naPALM). The molecule numbers could then be related to the cluster sizes in the rendered pointillist images (Fig. 5C). This analysis showed that gephyrin clusters were on average somewhat bigger in spinal cord slices ( $0.061 \pm 0.005 \mu\text{m}^2$ ,  $n = 44$  from 3 slices) than in cultured neurons ( $0.048 \pm 0.002 \mu\text{m}^2$ ,  $n = 115$ , 11 cells, 3 experiments). However, this difference was not very pronounced, and was partly due to the fact that gephyrin clusters in slices were more often composed of sub-domains that may be considered as separate entities. This fits with previous

observations that the size of spinal cord synapses varies over a wide range, and that larger PSDs have more complex shapes (Triller et al., 1985; Lushnikova et al., 2011). However, we did observe strong differences as regards the molecule density of gephyrin clusters in adult slices ( $12642 \pm 749$  molecules/ $\mu\text{m}^2$ ) as opposed to cultured neurons ( $5054 \pm 260$  molecules/ $\mu\text{m}^2$ ), suggestive of a greater maturity of inhibitory PSDs in native tissue.

We thus looked at the temporal profile of gephyrin clustering during postnatal development. The number of mRFP-gephyrin clusters in 1  $\mu\text{m}$  thick cortex and spinal cord slices increased with age, reaching about 0.1 clusters/ $\mu\text{m}^2$  in adult grey matter (Fig. S2A). Surprisingly, we found that the number of mRFP-gephyrin molecules at these clusters differed substantially between mature synapses in spinal cord and cortex (at 6 months), with a mean of  $393 \pm 19$  and  $133 \pm 10$  molecules, respectively ( $n_{\text{spc}} = 427$  and  $n_{\text{cor}} = 264$  clusters from  $\geq 6$  slices; Fig. S2B). Thus, in addition to temporal changes, other factors clearly regulate gephyrin scaffolds. Speculating that the inhibitory receptor types expressed in spinal cord and cortex may have something to do with this, we visualised endogenous GlyR $\alpha$ 1 subunits in 6 month-old cortex and spinal cord slices by immunohistochemistry (Fig. 5D). Whereas no GlyRs were detected in cortex, many of the PSDs in spinal cord were positive for GlyR $\alpha$ 1. The glycinergic synapses in the spinal cord were those with the highest number of clustered mRFP-gephyrin molecules ( $588 \pm 30$  molecules,  $n = 216$  clusters; Fig. 5E). In contrast, spinal cord synapses with little or no GlyR $\alpha$ 1 had inhibitory scaffolds that were more similar to those in the cortex ( $193 \pm 12$  gephyrin molecules,  $n = 211$ ; and  $133 \pm 10$ ,  $n = 264$ , respectively). Similarly, the sizes and the packing densities of gephyrin clusters were substantially higher in GlyR-containing spinal cord synapses ( $0.062 \pm 0.004 \mu\text{m}^2$ ,  $8771 \pm 576$  molecules/ $\mu\text{m}^2$ ,  $n = 59$  clusters from 4 slices) than in cortex ( $0.036 \pm 0.003 \mu\text{m}^2$ ,  $4460 \pm 360$  molecules/ $\mu\text{m}^2$ ,  $n = 28$  clusters from 3 slices; Fig. 5F). These observations suggest that receptor-scaffold interactions play a decisive role for the assembly and stability of inhibitory synaptic scaffolds.

#### Activity-dependent competition of endogenous GlyRs and GABA<sub>A</sub>Rs for synaptic binding sites

Spinal cord neurons express both GlyRs and GABA<sub>A</sub>Rs that bind to a common site on gephyrin (Maric et al., 2011; Kowalczyk et al., 2013). In order to dissect the relationship between these two types of receptors, we measured their concentrations at inhibitory synapses by dual immunolabelling in mRFP-gephyrin KI spinal cord cultures (Fig. 6A). Endogenous gephyrin

molecules were quantified through decay recordings, and the synaptic clusters were then binned according to gephyrin number (Fig. 6B). In line with our observations in spinal cord slices, the synaptic levels of GlyRs correlated with the number of gephyrin molecules, as did the GABA<sub>A</sub>R levels (Fig. 6C,D). However, the synaptic accumulation of GABA<sub>A</sub>R $\alpha$ 2 was significantly reduced in spinal cord neurons that had been treated for 48 h with 1  $\mu$ M tetrodotoxin (TTX) to block action potentials and to minimise the network activity in the cultures (Kilman et al., 2002).

Since TTX had no obvious effect on the synaptic enrichment of GlyRs (Fig. 6C), we expected the activity-dependent regulation to be most pronounced at pure GABAergic synapses. As a measure of GlyR occupancy of inhibitory PSDs we calculated the ratio of GlyR $\alpha$ 1 fluorescence / mRFP-gephyrin number and sorted the clusters accordingly (Fig. 6E). This analysis revealed that the inhibitory PSDs with the lowest GlyR occupancy (1<sup>st</sup> and 2<sup>nd</sup> quartiles) had the highest GABA<sub>A</sub>R $\alpha$ 2 occupancy, and were most affected by activity blockade with TTX (Fig. 6F). Together, these data show that the number of synaptic binding sites controls the receptor levels at inhibitory PSDs and that activity-dependent processes regulate the competition between receptors.

#### Quantification of GlyR binding sites at synaptic gephyrin clusters

The close correspondence of receptors and gephyrin scaffolds at inhibitory synapses both in terms of spatial organisation (Fig. 2 & 3) as well as protein numbers (Fig. 5 & 6) begs the question whether a stable stoichiometry exists between the number of gephyrin molecules and the available receptor binding sites. To quantify the absolute number of GlyR binding sites at inhibitory synapses, we transfected spinal cord KI cultures with a membrane construct containing the gephyrin-binding domain of GlyR $\beta$ . The  $\beta$ -loop-TMD-Dendra2 construct co-localises with mRFP-gephyrin clusters and has the ability to replace endogenous GlyRs (Specht et al., 2011). The mRFP and Dendra2 fluorophores were quantified by sequential bleaching in the red (mRFP) and green (Dendra2) channels. This revealed an average occupancy of  $\sim$ 0.5  $\beta$ -loop constructs per synaptic gephyrin molecule, a ratio that varied from cell to cell and that reached a maximum of  $\sim$ 1.1 in neurons with the highest  $\beta$ -loop-TMD-Dendra2 expression (Fig. 7A). In spinal cord neurons, however, the presence of endogenous GlyRs and GABA<sub>A</sub>Rs needs to be taken into account. The counting of receptor binding sites was therefore repeated in COS-7 cells, a reduced cellular model devoid of endogenous inhibitory receptors. In this cell line, the co-expression of  $\beta$ -loop-TMD-

Dendra2 and mRFP-gephyrin created small clusters that displayed a linear dependence between  $\beta$ -loops and gephyrin molecules (slope  $\sim 1.4$ ; Fig. 7B). These findings suggest that  $\beta$ -loop-TMD-Dendra2 can replace endogenous receptors and occupy all synaptic binding sites, and that all gephyrin molecules at synapses can contribute to the immobilisation of inhibitory receptors.

## **Discussion**

### Quantitative nanoscopy: building a realistic model of the synaptic structure

The performance of the synapse as a signalling device is largely a function of its molecular composition; it is determined by the number of synaptic components and their place within the synaptic structure. The central concept of this study was to exploit the inherent property of single molecule imaging to detect fluorophores one at a time, in order to extract ultra-structural as well as quantitative data on the gephyrin scaffold at inhibitory synapses in spinal cord neurons. Using a range of single molecule-based imaging approaches we have thus gained access to new types of information that afford a more realistic view of the organisation and composition of inhibitory PSDs (Table 1).

The common basis of quantitative imaging techniques is to calibrate fluorescence intensity units against a known concentration or number of fluorophores such as GFP. The intensities of individual fluorophores are easily measured in single molecule experiments, and can be used to convert units of fluorescence into numbers of molecules (Ulbrich and Isacoff, 2007; Durisic et al., 2012). Applying this methodology, we analysed the photobleaching intensity steps of converted Dendra2 fluorophores to access absolute molecule numbers. The summed peaks of a train of photoconversion pulses gave the total number of Dendra2-gephyrin molecules in a discrete gephyrin cluster. In other words, we have quantified the number of photoconversion events until depletion, rather than the number of fluorophore detections. The rationale of our approach was that the blinking of fluorescent proteins impedes the simple counting of the number of detections in PALM recordings. The quantitative interpretation of PALM data can in principle be achieved by identifying bursts of detections arising from the same fluorophore and by reducing these detections to a single data point. However, this type of analysis is limited to fluorophore densities of up to 1000 molecules/ $\mu\text{m}^2$  (Annibale et al., 2011), much lower than those present at synaptic gephyrin clusters ( $\sim 5000$ - $10000$  molecules/ $\mu\text{m}^2$ ).

To validate our molecule counting strategy we also developed another quantitative approach that consists in bleaching a population of fluorophores without photoconversion. This technique is equally applicable to non-converted Dendra2 fluorophores and to conventional fluorophores such as mRFP. In short, decay traces of recombinant Dendra2-gephyrin or endogenous mRFP-gephyrin clusters were fitted to extract the area under the curve (total cluster fluorescence) and the decay time (fluorophore lifetime). The intensity of single fluorophores was given by blinking events in the later stages of the recording. From these three parameters the number of fluorophores in the cluster was calculated (see methods). In addition, the blinking of fluorophores at the end of the movie can be used for the reconstruction of PALM-like nanoscopic images, provided the quantum yield is sufficiently high to achieve a good localisation accuracy (as is the case for mRFP). We refer to this type of imaging as non-activated PALM (naPALM). It should be noted that the bleaching of the fluorophore population reduces the sampling of the structure, which can compromise the spatial resolution. We have therefore used naPALM only to measure the overall size of mRFP-gephyrin clusters, and relied on classical PALM and STORM imaging for ultra-structural information.

In summary, the quantitative approaches presented here are appropriate for counting large numbers of fluorophores within dense structures. The resulting data are to be seen as estimates that do not account for a number of factors. The efficacy of fluorescent protein folding, for example, has not been considered. Previous studies have shown that ~80% of fluorophores are functional (Ulbrich and Isacoff, 2007). If applied to our data, this correction would raise the average gephyrin numbers at inhibitory synapses from 200 to 250 molecules. These values are comparable to the number of scaffold proteins at excitatory synapses (e.g. 200-300 copies of PSD-95; discussed in Specht and Triller, 2008).

#### The planar structure and organisation of inhibitory PSDs

Several lines of evidence indicate that gephyrin clusters are two-dimensional structures underneath the plasma membrane. EM data have shown that the PSDs have a thickness of approximately 33 nm (Carlin et al., 1980). Immuno-EM has further revealed that gephyrin molecules lie at a relatively constant distance from the synaptic membrane (Triller et al., 1985). More specifically, different epitopes are detected at different distances – gold particles associated with the antibodies mAb7a (gephyrin C-domain) and mAb5a are found at 22 nm and at 30 nm, respectively– suggesting that

gephyrin molecules are not arranged strictly parallel to the plasma membrane. In order to explore the three-dimensional organisation of the gephyrin scaffold we have implemented dual-colour 3D-PALM/STORM imaging using adaptive optics. Previous STORM imaging with an astigmatic lens has mapped the vertical organisation of excitatory synapses, showing a close correspondence with EM data (Dani et al., 2010). With a deformable mirror as opposed to an astigmatic lens in the imaging path, the deformation of the PSF can be adjusted to optimise the signal detection and to set the dynamic range along the z-axis (Izeddin et al., 2012). Using this approach, we measured the distance of the gephyrin scaffold to the synaptic cleft. The average distance of the N-terminus of gephyrin to the extracellular mAb2b epitope of GlyR $\alpha$ 1 was 44 nm. This comprises the mEos2 tag (estimated at 4 nm, similar to GFP; Ormo et al., 1996), the distance of gephyrin to the membrane (~10 nm; Triller et al., 1986), the membrane and extracellular domains of the GlyR (~11 nm as member of the Cys-loop superfamily; Unwin, 2005) and the two antibodies (~10 nm each; Triller et al., 1986). These molecular lengths add up to 45 nm, in good agreement with our direct observation. The apparent thickness of the gephyrin cluster itself was in the order of 100 nm, at the limit of resolution set by our 3D-PALM imaging conditions.

Further support for the planar molecular structure comes from our quantitative analysis of gephyrin clusters. We have shown that the gephyrin scaffold provides about as many receptor binding sites as there are gephyrin molecules in the cluster (Table 1). This means that all gephyrin molecules must be oriented such that they can interact with receptors in the synaptic membrane. Whether or not the binding sites are actually occupied depends on the number of available binding partners and their affinities (see below). Moreover, we found a linear correlation between endogenous mRFP-gephyrin fluorescence (i.e. molecule number) and gephyrin immunolabelling (i.e. cluster surface; antibody mAb7a;  $R^2 = 0.82$ , data not shown). Both these observations lend support to a model in which all gephyrin monomers within the cluster are exposed equally towards the synaptic membrane as well as the cytoplasm.

Based on the oligomerisation properties of gephyrin there exists a general consensus that the lateral organisation of the gephyrin scaffold is that of a hexagonal network (Kneussel and Betz, 2000; Schwarz et al., 2001; Sola et al., 2001; Xiang et al., 2001; Sola et al., 2004). Our experiments revealed synaptic gephyrin densities as high as 10000 molecules/ $\mu\text{m}^2$  at mature spinal cord synapses *in vivo*, which corresponds to a two-dimensional spacing in the order of 10 nm between

gephyrin monomers. However, gephyrin molecules were packed less densely in the cortex and in dissociated spinal cord cultures ( $\sim 5000$  molecules/ $\mu\text{m}^2$ ), indicating that the organisation of the gephyrin scaffold can be somewhat irregular (Sola et al., 2004), and depend on receptor-gephyrin interactions as well as synapse maturity. Denser gephyrin packing is likely accompanied by an increased stability of the synaptic scaffold, as seen in the developmental reduction of the gephyrin exchange kinetics shown in a recent study (Vlachos et al., 2012). Yet, PALM imaging revealed that the internal structure of gephyrin clusters has an additional level of organisation. Many of the larger gephyrin clusters are composed of sub-domains that are separated by areas with low gephyrin concentrations. Inhibitory synapses with different levels of complexity have also been observed by EM (Triller and Korn, 1982). That some synapses with segmented PSDs are apposed to separate pools of synaptic vesicles means that they may be considered as independent entities (Lushnikova et al., 2011). Accordingly, dynamic PALM imaging revealed that the sub-clusters of gephyrin change their relative positions on a time scale of minutes. These rearrangements may correspond with the splitting and merging of gephyrin clusters as observed frequently during time-lapse imaging (Dobie and Craig, 2011).

#### The gephyrin scaffold as a dynamic platform for competing inhibitory receptors

The morphology of inhibitory PSDs appears to play a role in the homeostatic regulation of inhibitory synapses. Both size and complexity of inhibitory PSDs increase in response to excitatory synaptic plasticity (Nusser et al., 1998; Bourne and Harris, 2011; Lushnikova et al., 2011). This is likely paralleled by functional changes, since the size of the PSD determines the receptor levels at inhibitory synapses (Nusser et al., 1997; Lim et al., 1999; Kasugai et al., 2010). In agreement with these findings, our PALM/STORM data show a close match between the distribution of gephyrin and GlyRs at spinal cord synapses. The 3D data in particular illustrate the correspondence between mEos2-gephyrin clusters and GlyR localisation. The comparison of endogenous receptor densities (1250 pentameric GABA<sub>A</sub>R complexes  $\mu\text{m}^{-2}$  in cerebellar stellate cells; Nusser et al., 1997) and the measured gephyrin densities ( $\sim 5000$   $\mu\text{m}^{-2}$  at GlyR $\alpha 1$ -negative cortical synapses) suggests that the receptors may actually occupy a high proportion of the available binding sites at central GABAergic synapses, assuming the simultaneous binding of several subunits per receptor complex.

Does this imply that changes in the clustering of gephyrin are necessarily followed by alterations in receptor numbers at inhibitory synapses? The parallel changes of gephyrin and GlyR clustering



downstream of integrin signalling suggest that this may be so (Charrier et al., 2010). Along the same line, our data show that GlyR and GABA<sub>A</sub>R levels increase with the number of clustered gephyrin molecules at spinal cord synapses. Regulatory processes at GABAergic synapses may also affect GABA<sub>A</sub>Rs and gephyrin levels alike (Bannai et al., 2009; Papadopoulos and Soykan, 2011), however, the sequence of these events is less clear, since there exists a reciprocal stabilisation between GABA<sub>A</sub>Rs and gephyrin (discussed in Fritschy et al., 2008). This is reminiscent of our observation that the formation of gephyrin clusters in COS-7 cells depends on the presence of membrane constructs with a gephyrin-binding sequence. Under these conditions, gephyrin and the membrane proteins were found to associate in a stable stoichiometry.

On the other hand, mechanisms that alter the affinity of receptor-gephyrin binding have the potential to uncouple gephyrin clustering and receptor numbers. For instance, activity deprivation with TTX reduced GABA<sub>A</sub>R $\alpha$ 2 levels at spinal cord synapses in line with previous observations (Kilman et al., 2002), whereas gephyrin numbers and GlyR $\alpha$ 1 levels were remarkably resilient to the treatment. Receptor-gephyrin affinities can be regulated by phosphorylation of GlyRs or GABA<sub>A</sub>Rs at their gephyrin-binding sites (Mukherjee et al., 2011; Specht et al., 2011) or by post-translational modifications of gephyrin itself (Zita et al., 2007). Since these mechanisms are independent of gephyrin clustering as such, the synaptic scaffold can act as a rather stable platform for the immobilisation of inhibitory receptors that compete for existing binding sites. Consequently the membrane construct  $\beta$ -loop-TMD-Dendra2 accumulates at gephyrin clusters in a dose-dependent manner, likely through the displacement of endogenous receptor complexes at spinal cord synapses (Specht et al., 2011). At high expression levels, we observed the saturation of binding sites by  $\beta$ -loop-TMD-Dendra2 (occupancy  $\sim$ 1.1).

It is well known that the GlyR  $\beta$ -loop binds to the gephyrin E-domain with high affinity (Herweg and Schwarz, 2012 and references cited therein). An initial model suggested a 1:1 stoichiometry between pentameric GlyR complexes and gephyrin (Kirsch and Betz, 1995). However, the presence of two  $\beta$  subunits per GlyR complex (Durisic et al., 2012) makes it much more attractive that the receptors interact with the gephyrin scaffold via both binding sites, either within the same gephyrin trimer (Fritschy et al., 2008) or by crosslinking neighbouring trimers (Sola et al., 2004), thus attaining a higher avidity for the gephyrin scaffold. This model is consistent with the observation

that glycinergic spinal cord synapses are very dense and stable molecular assemblies that are largely insensitive to the blockade of excitatory activity by TTX. Consequently, synaptic GlyRs display a confined diffusion within gephyrin clusters, only exchanging between sub-domains of the cluster on a slow time scale of tens of seconds. Given recent advances in single molecule imaging it is now foreseeable to directly measure absolute receptor fluxes at synapses as well as dynamic transitions between different steady states, providing an access to the dynamic equilibrium of molecular interactions in living cells.

## **Experimental procedures**

### Plasmids

The coding sequence of rat gephyrin (GenBank X66366, splice variant P1) was fused at its N-terminus to Dendra2 (Clontech #632546), mEos2 (GenBank FJ707374) and mRFP (GenBank AF506027) via a GSLGG linker, to generate the plasmids Dendra2-gephyrin, mEos2-gephyrin and mRFP-gephyrin. Plasmid  $\beta$ -loop-TMD-Dendra2 consists of the cytoplasmic M3-M4 loop of mouse GlyR $\beta$  (residues N334-A454 excluding signal peptide, UniProt ID P48168) fused to a single transmembrane domain and extracellular Dendra2 (in analogy to  $\beta$ L<sup>wt</sup>-TMD-pHluorin; Specht et al., 2011). The fusion constructs were cloned in a eukaryotic expression vector derived from pEGFP-N1 (Clontech) with a partial deletion of the CMV promoter.

### Cell culture and transfection

Spinal cord dissociated neuron cultures were prepared from Sprague-Dawley rats (at E14) and from homozygous mRFP-gephyrin knock-in (KI) mice (at E13) as described (Calamai et al., 2009). Neurons were plated at a density of  $6 \times 10^4/\text{cm}^2$  on 18 mm coverslips (thickness 0.13-0.16 mm), cultured in neurobasal medium containing B-27, 2 mM glutamine, 5 U/ml penicillin and 5  $\mu\text{g}/\text{ml}$  streptomycin at 36°C and 5% CO<sub>2</sub>, transfected with 0.5  $\mu\text{g}$  plasmid DNA per coverslip using Lipofectamine 2000, and used for experiments on the following day (at DIV12-24). COS-7 cells were grown on coverslips in DMEM containing 10% FCS, and co-transfected with  $\beta$ -loop-TMD-Dendra2 and mRFP-gephyrin in a stoichiometry of 1:4 on the day prior to the experiments using FuGENE 6.

### Sample preparation

Cell cultures were fixed for 10 min in 0.1 M sodium phosphate pH 7.4 containing 4% PFA and 1% sucrose, rinsed and imaged in PBS pH 7.4 (PALM and fluorophore counting). For PALM and STORM imaging, fiducial markers (TetraSpeck microspheres, 100 nm diameter, Invitrogen #T7279) were attached to the coverslips after fixation. For immunolabelling, fixed neurons were permeabilised with 0.25% Triton X-100 where necessary, and labelled in PBS containing 3% BSA with antibodies against extracellular epitopes of GlyR $\alpha$ 1 (Synaptic Systems, mAb2b, #146111, 1:200-400 dilution) and GABA<sub>A</sub>R $\alpha$ 2 (Synaptic Systems, #224103, 1:400), the phosphorylated C-domain of gephyrin (Synaptic Systems, mAb7a, #147011, 1:500; Kuhse et al., 2012) or the N-terminus of bassoon (sap7f, 1:500; tom Dieck et al., 1998) followed by Alexa Fluor 647 or 488-tagged secondary antibodies (Invitrogen, 1:250-500). dSTORM was done in PBS pH 7.4 containing 10% glucose, 50 mM  $\beta$ -mercaptoethylamine, 0.5 mg/ml glucose oxidase and 40  $\mu$ g/ml catalase, degassed with N<sub>2</sub> (Izeddin et al., 2011).

Spinal cord and cerebral cortex sections were prepared from mRFP-gephyrin knock-in mice. Male animals of 1 week to 6 months of age were perfused intracardially with 4% PFA and 0.1% glutaraldehyde in PBS pH 7.4. Spinal cords (thoracic dorsal horn) and cortices (non-superficial layers of the frontal lobe) were dissected, post-fixed with 4% PFA in PBS, cut into 1 mm segments and incubated over night in 2.3 M sucrose in PBS at 4°C. The tissue was frozen in liquid nitrogen and sliced at -80°C with a cryo-ultramicrotome (Leica Ultracut EM UC6). Slices of 0.5 or 1  $\mu$ m thickness were placed on glass coverslips, immunolabelled if required, and imaged in PBS.

### Live imaging

Dynamic imaging (live PALM, SPT-QD and fluorophore counting) was done at 35°C in imaging medium (MEM without phenol red, 33 mM glucose, 20 mM HEPES, 2 mM glutamine, 1 mM sodium pyruvate, B-27). For SPT-QD of endogenous GlyRs (Specht et al., 2011), neurons were sequentially incubated with antibodies against GlyR $\alpha$ 1 (mAb2b; 1:1000, 4 min), biotinylated goat anti-mouse Fab fragments (Jackson Immunoresearch; 1:1000, 4 min) and streptavidin-conjugated QDs emitting at 705 nm (Invitrogen, #Q10161MP, diameter ~25 nm; 1 nM, 1 min).

### PALM and STORM

Single molecule imaging was carried out as described (Izeddin et al., 2011) on an inverted Nikon Eclipse Ti microscope with a 100x oil-immersion objective (N.A. 1.49), an additional 1.5x lens and an Andor iXon EMCCD camera (image pixel size 107 nm), using specific lasers for PALM

imaging of Dendra2 and mEos2 (405 and 561 nm), STORM of Alexa Fluor 647 (532 and 639 nm), and photobleaching of pre-converted Dendra2 fluorophores (491 nm). Movies of  $\leq 6 \times 10^4$  frames were acquired at frame rates of 20 ms (live) and 50 ms (fixed samples). The z-position was maintained during acquisition by a Nikon perfect focus system. Dual-colour STORM/PALM imaging was done sequentially. Simultaneous PALM and SPT-QD was carried out with a Photometrics dual-view system, using 561 nm laser excitation for both the QDs and the converted mEos2 fluorophores. The emitted light was separated with a 633 nm dichroic and filtered for mEos2 (593/40 nm) and QD705 (692/40 nm). The SPT-QD acquisitions were kept to  $\leq 160$  s (8000 frames of 20 ms) to exclude the spectral shift (*blueing*) of QDs (Hoyer et al., 2011). Conventional fluorescence imaging was done with a mercury lamp and specific filter sets for the detection of pre-converted Dendra2, mEos2 and Alexa 488 (excitation 485/20 nm, emission 525/30 nm), mRFP (ex. 560/25, em. 607/36) and Alexa 647 (ex. 650/13, em. 684/24).

### PALM/STORM image reconstruction

Single molecule localisation and 2D-image reconstruction was done as described (Izeddin et al., 2011), by fitting the point-spread function (PSF) of spatially separated fluorophores to a 2D Gaussian distribution. In fixed cell experiments, 100 nm TetraSpeck beads were used to correct the x/y-drift during acquisition (generally  $< 200$  nm), with a sliding window of 100 frames. In live PALM and naPALM experiments, we corrected the positions of fluorophore detections by the relative movement of the synaptic cluster itself, i.e. by calculating the centre of mass of the cluster throughout the acquisition using a partial reconstruction of 2000 image frames with a sliding window. PALM and STORM images were rendered by superimposing the coordinates of single molecule detections, which were represented with 2D Gaussian curves of unitary intensity and standard deviation  $\sigma$  representing the localisation accuracy (10 nm). Gephyrin cluster sizes were measured in reconstructed 2D images through cluster segmentation and by counting the pixels above the segmentation threshold forming a single cluster (Fig. 1B,5C). Alternatively, cluster areas were measured directly from super-resolution localisations based on relative localisation densities (ViSP software, El Beheiry and Dahan, under review; data shown in Fig. 5F).

### 3D-PALM/STORM

Three-dimensional PALM/STORM imaging was performed using adaptive optics (AO) to induce 2D astigmatism to the PSF of single molecules (Izeddin et al., 2012). With PSF shaping, the axial

symmetry of the signal was broken, giving access to the z-position of individual fluorophores in addition to the x/y-coordinates. The experimental set-up was as described above, with the addition of a MicAO system (Imagine Optic) in the emission pathway. The AO system was used to correct aberrations of the PSF and to induce a controlled degree of astigmatism (amplitude 0.06  $\mu\text{m}$ ). For z-axis calibration, 100 nm TetraSpeck beads were imaged with the help of a piezo nanopositioning stage (Nano-Z500, Mad City Labs) over a range of 1  $\mu\text{m}$  with a step size of 6 nm. Calibration curves were taken for the 593/40 nm and 684/24 emission wavelengths for each experiment. We then proceeded with the STORM and PALM acquisitions. Astigmatic PSFs were analysed using an asymmetric 2D Gaussian fit. The centre position of the fit represented the x/y-coordinates of the fluorophores, whereas the difference of the length and width of the fitted PSFs ( $\Delta w = w_x - w_y$ ) was mapped against the calibration curves in order to retrieve the z-positions of single fluorophores. Localised molecules were rendered as a point cloud in a 3D scatter plot for both colour channels (ViSP software, El Beheiry and Dahan, under review). Point cloud densities were calculated to illustrate the relative molecular concentrations of gephyrin and GlyRs, whereas surface rendering served to further depict the morphology and orientation of the synaptic clusters.

### Quantitative single molecule imaging

**Pulsed photoconversion:** To quantify the number of photoconverted fluorophores (Dendra2-gephyrin), 100 ms pulses of 405 nm laser were applied every 30 s, during continuous imaging with the 561 nm laser ( $\leq 4 \times 10^4$  frames at 50 ms). Dendra2 bleaching steps were identified in the decay traces of the conversion pulses of individual gephyrin clusters to measure the mean intensity of single fluorophores above the background offset. The sum of the pulse peak intensities  $n_i$  was then used to calculate the total number of molecules in the same cluster:  $N = \sum n_i$

**Photobleaching and single fluorophore detection:** Gephyrin clusters were photobleached with laser illumination (mRFP-gephyrin with 561 nm and the non-converted form of Dendra2 with 491 nm;  $\leq 10^4$  frames at 20-50 ms). The decay traces of individual clusters were corrected for the background noise offset and fitted with a double exponential equation to extract the weighted decay constant  $\tau_w$  (from the two characteristic decay times  $\tau_1$  and  $\tau_2$  and their amplitudes  $a_1$  and  $a_2$ ) as well as the integrated cluster intensity  $A$  (area under the curve). Single fluorophore blinking events were detected at the end of the movie (typically in frames 5000-10000), and their mean intensity  $I$  measured for each cluster. The total fluorophore number  $N$  of the cluster was then calculated

according to the formula:  $N = A / (I \times \tau_w)$ . For dual-colour quantification, decay recordings were acquired first for mRFP followed by Dendra2, since excitation at 561 nm did not affect the non-converted form of Dendra2.

**Conversion of fluorescence intensities to molecule numbers:** The calculated fluorophore numbers of individual gephyrin clusters (from the pulsed photoconversion or the fluorescence decay method) were equated to the fluorescence intensity of the same clusters in images taken with the mercury lamp (background-corrected integrated cluster intensity). This resulted in a conversion factor  $\varphi$  (fluorescence intensity / molecule) that could be applied to any structure visualised in conventional fluorescence images, provided identical imaging conditions were maintained.

## Acknowledgements

The authors thank Alain Bessis, Yasmine Cantaut-Belarif and Andréa Dumoulin (IBENS, Paris), as well as Christophe Zimmer and Mickaël Lelek (Institut Pasteur, Paris) for technical help. This project was funded by the Fondation Pierre-Gilles de Gennes through a research contract with Nikon France, the Institut pour la Recherche sur la Moelle Épinière et l'Encéphale (IRME), and by grants TRIDIMIC and MorphoSynDiff from the Agence Nationale pour la Recherche (ANR). CGS acknowledges grant Lamonica, and II the Netherlands Organisation for Scientific Research (NWO) for financial support. Author contributions: CGS, II, MD and AT designed the experiments; CGS, II, PCR, PR and MEB did the experiments and analysed the data; CGS and II wrote the manuscript. The authors declare no conflict of interest.

## References

- Annibale, P., Vanni, S., Scarselli, M., Rothlisberger, U., and Radenovic, A. (2011). Quantitative photo activated localization microscopy: unraveling the effects of photoblinking. *PLoS One* *6*, e22678.
- Bannai, H., Levi, S., Schweizer, C., Inoue, T., Launey, T., Racine, V., Sibarita, J.B., Mikoshiba, K., and Triller, A. (2009). Activity-dependent tuning of inhibitory neurotransmission based on GABAAR diffusion dynamics. *Neuron* *62*, 670-682.
- Bausen, M., Weltzien, F., Betz, H., and O'Sullivan, G.A. (2010). Regulation of postsynaptic gephyrin cluster size by protein phosphatase 1. *Mol Cell Neurosci* *44*, 201-209.
- Bourne, J.N., and Harris, K.M. (2011). Coordination of size and number of excitatory and inhibitory synapses results in a balanced structural plasticity along mature hippocampal CA1 dendrites during LTP. *Hippocampus* *21*, 354-373.
- Calamai, M., Specht, C.G., Heller, J., Alcor, D., Machado, P., Vannier, C., and Triller, A. (2009). Gephyrin oligomerization controls GlyR mobility and synaptic clustering. *J Neurosci* *29*, 7639-7648.
- Carlin, R.K., Grab, D.J., Cohen, R.S., and Siekevitz, P. (1980). Isolation and characterization of postsynaptic densities from various brain regions: enrichment of different types of postsynaptic densities. *J Cell Biol* *86*, 831-845.
- Charrier, C., Machado, P., Tweedie-Cullen, R.Y., Rutishauser, D., Mansuy, I.M., and Triller, A. (2010). A crosstalk between beta1 and beta3 integrins controls glycine receptor and gephyrin trafficking at synapses. *Nat Neurosci* *13*, 1388-1395.
- Dani, A., Huang, B., Bergan, J., Dulac, C., and Zhuang, X. (2010). Superresolution imaging of chemical synapses in the brain. *Neuron* *68*, 843-856.
- Dobie, F.A., and Craig, A.M. (2011). Inhibitory synapse dynamics: coordinated presynaptic and postsynaptic mobility and the major contribution of recycled vesicles to new synapse formation. *J Neurosci* *31*, 10481-10493.
- Durisic, N., Godin, A.G., Wever, C.M., Heyes, C.D., Lakadamyali, M., and Dent, J.A. (2012). Stoichiometry of the human glycine receptor revealed by direct subunit counting. *J Neurosci* *32*, 12915-12920.
- Ehrensperger, M.V., Hanus, C., Vannier, C., Triller, A., and Dahan, M. (2007). Multiple association states between glycine receptors and gephyrin identified by SPT analysis. *Biophys J* *92*, 3706-3718.
- Fritschy, J.M., Harvey, R.J., and Schwarz, G. (2008). Gephyrin: where do we stand, where do we go? *Trends Neurosci* *31*, 257-264.
- Hanus, C., Ehrensperger, M.V., and Triller, A. (2006). Activity-dependent movements of postsynaptic scaffolds at inhibitory synapses. *J Neurosci* *26*, 4586-4595.
- Herweg, J., and Schwarz, G. (2012). Splice-specific glycine receptor binding, folding, and phosphorylation of the scaffolding protein gephyrin. *J Biol Chem* *287*, 12645-12656.
- Hoyer, P., Staudt, T., Engelhardt, J., and Hell, S.W. (2011). Quantum dot blueing and blinking enables fluorescence nanoscopy. *Nano Lett* *11*, 245-250.
- Huang, B., Wang, W., Bates, M., and Zhuang, X. (2008). Three-dimensional super-resolution imaging by stochastic optical reconstruction microscopy. *Science* *319*, 810-813.
- Izeddin, I., Specht, C.G., Lelek, M., Darzacq, X., Triller, A., Zimmer, C., and Dahan, M. (2011). Super-resolution dynamic imaging of dendritic spines using a low-affinity photoconvertible actin probe. *PLoS One* *6*, e15611.
- Izeddin, I., El Beheiry, M., Andilla, J., Ciepielewski, D., Darzacq, X., and Dahan, M. (2012). PSF shaping using adaptive optics for three-dimensional single-molecule super-resolution imaging and tracking. *Opt Express* *20*, 4957-4967.
- Kasugai, Y., Swinny, J.D., Roberts, J.D., Dalezios, Y., Fukazawa, Y., Sieghart, W., Shigemoto, R., and Somogyi, P. (2010). Quantitative localisation of synaptic and extrasynaptic GABAA receptor subunits on hippocampal pyramidal cells by freeze-fracture replica immunolabelling. *Eur J Neurosci* *32*, 1868-1888.

- Kilman, V., van Rossum, M.C., and Turrigiano, G.G. (2002). Activity deprivation reduces miniature IPSC amplitude by decreasing the number of postsynaptic GABA(A) receptors clustered at neocortical synapses. *J Neurosci* 22, 1328-1337.
- Kirsch, J., and Betz, H. (1995). The postsynaptic localization of the glycine receptor-associated protein gephyrin is regulated by the cytoskeleton. *J Neurosci* 15, 4148-4156.
- Kneussel, M., and Betz, H. (2000). Clustering of inhibitory neurotransmitter receptors at developing postsynaptic sites: the membrane activation model. *Trends Neurosci* 23, 429-435.
- Kowalczyk, S., Winkelmann, A., Smolinsky, B., Forstera, B., Neundorf, I., Schwarz, G., and Meier, J.C. (2013). Direct binding of GABA(A) receptor beta2 and beta3 subunits to gephyrin. *Eur J Neurosci* 37, 544-554.
- Kuhse, J., Kalbouneh, H., Schlicksupp, A., Mukusch, S., Nawrotzki, R., and Kirsch, J. (2012). Phosphorylation of gephyrin in hippocampal neurons by cyclin-dependent kinase CDK5 at Ser-270 is dependent on collybistin. *J Biol Chem* 287, 30952-30966.
- Lim, R., Alvarez, F.J., and Walmsley, B. (1999). Quantal size is correlated with receptor cluster area at glycinergic synapses in the rat brainstem. *J Physiol* 516 ( Pt 2), 505-512.
- Lushnikova, I., Skibo, G., Muller, D., and Nikonenko, I. (2011). Excitatory synaptic activity is associated with a rapid structural plasticity of inhibitory synapses on hippocampal CA1 pyramidal cells. *Neuropharmacology* 60, 757-764.
- Maric, H.M., Mukherjee, J., Tretter, V., Moss, S.J., and Schindelin, H. (2011). Gephyrin-mediated gamma-aminobutyric acid type A and glycine receptor clustering relies on a common binding site. *J Biol Chem* 286, 42105-42114.
- Mukherjee, J., Kretschmannova, K., Gouzer, G., Maric, H.M., Ramsden, S., Tretter, V., Harvey, K., Davies, P.A., Triller, A., Schindelin, H., and Moss, S.J. (2011). The residence time of GABA(A)Rs at inhibitory synapses is determined by direct binding of the receptor alpha1 subunit to gephyrin. *J Neurosci* 31, 14677-14687.
- Nusser, Z., Cull-Candy, S., and Farrant, M. (1997). Differences in synaptic GABA(A) receptor number underlie variation in GABA mini amplitude. *Neuron* 19, 697-709.
- Nusser, Z., Hajos, N., Somogyi, P., and Mody, I. (1998). Increased number of synaptic GABA(A) receptors underlies potentiation at hippocampal inhibitory synapses. *Nature* 395, 172-177.
- Ormo, M., Cubitt, A.B., Kallio, K., Gross, L.A., Tsien, R.Y., and Remington, S.J. (1996). Crystal structure of the *Aequorea victoria* green fluorescent protein. *Science* 273, 1392-1395.
- Papadopoulos, T., and Soykan, T. (2011). The role of collybistin in gephyrin clustering at inhibitory synapses: facts and open questions. *Front Cell Neurosci* 5, 11.
- Rigo, J.M., Badiu, C.I., and Legendre, P. (2003). Heterogeneity of postsynaptic receptor occupancy fluctuations among glycinergic inhibitory synapses in the zebrafish hindbrain. *J Physiol* 553, 819-832.
- Schwarz, G., Schrader, N., Mendel, R.R., Hecht, H.J., and Schindelin, H. (2001). Crystal structures of human gephyrin and plant Cnx1 G domains: comparative analysis and functional implications. *J Mol Biol* 312, 405-418.
- Singer, J.H., and Berger, A.J. (1999). Contribution of single-channel properties to the time course and amplitude variance of quantal glycine currents recorded in rat motoneurons. *J Neurophysiol* 81, 1608-1616.
- Sola, M., Kneussel, M., Heck, I.S., Betz, H., and Weissenhorn, W. (2001). X-ray crystal structure of the trimeric N-terminal domain of gephyrin. *J Biol Chem* 276, 25294-25301.
- Sola, M., Bavro, V.N., Timmins, J., Franz, T., Ricard-Blum, S., Schoehn, G., Ruigrok, R.W., Paarmann, I., Saiyed, T., O'Sullivan, G.A., Schmitt, B., Betz, H., and Weissenhorn, W. (2004). Structural basis of dynamic glycine receptor clustering by gephyrin. *Embo J* 23, 2510-2519.
- Specht C.G., and Triller A. (2008). The dynamics of synaptic scaffolds. *Bioessays* 30, 1062-1074.
- Specht, C.G., Grunewald, N., Pascual, O., Rostgaard, N., Schwarz, G., and Triller, A. (2011). Regulation of glycine receptor diffusion properties and gephyrin interactions by protein kinase C. *EMBO J* 30, 3842-3853.
- tom Dieck, S., Sanmarti-Vila, L., Langnaese, K., Richter, K., Kindler, S., Soyke, A., Wex, H., Smalla, K.H., Kampf, U., Franzer, J.T., Stumm, M., Garner, C.C., and Gundelfinger, E.D. (1998). Bassoon, a novel zinc-



- finger CAG/glutamine-repeat protein selectively localized at the active zone of presynaptic nerve terminals. *J Cell Biol* *142*, 499-509.
- Triller, A., and Korn, H. (1982). Transmission at a central inhibitory synapse. III. Ultrastructure of physiologically identified and stained terminals. *J Neurophysiol* *48*, 708-736.
- Triller, A., Cluzeaud, F., Pfeiffer, F., Betz, H., and Korn, H. (1985). Distribution of glycine receptors at central synapses: an immunoelectron microscopy study. *J Cell Biol* *101*, 683-688.
- Triller, A., Cluzeaud, F., Pfeiffer, F., and Korn, H. (1986). Distribution and transmembrane organization of glycine receptors at central synapses: an immunocytochemical touch. In *Molecular aspects of neurobiology*, R. Levi Montalcini, P. Calissano, E.R. Kandel, and A. Maggi, eds. (Berlin, Heidelberg, Springer-Verlag), pp. 101-105.
- Tyagarajan, S.K., Ghosh, H., Yevenes, G.E., Nikonenko, I., Ebeling, C., Schwerdel, C., Sidler, C., Zeilhofer, H.U., Gerrits, B., Muller, D., and Fritschy, J.M. (2011). Regulation of GABAergic synapse formation and plasticity by GSK3beta-dependent phosphorylation of gephyrin. *Proc Natl Acad Sci U S A* *108*, 379-384.
- Tyagarajan, S.K., Ghosh, H., Yevenes, G.E., Imanishi, S.Y., Zeilhofer, H.U., Gerrits, B., and Fritschy, J.M. (2013). ERK and GSK3beta regulate gephyrin postsynaptic aggregation and GABAergic synaptic function in a calpain-dependent mechanism. *J Biol Chem* *288*, 9634-9647.
- Ulbrich, M.H., and Isacoff, E.Y. (2007). Subunit counting in membrane-bound proteins. *Nat Methods* *4*, 319-321.
- Unwin, N. (2005). Refined structure of the nicotinic acetylcholine receptor at 4A resolution. *J Mol Biol* *346*, 967-989.
- Vlachos, A., Reddy-Alla, S., Papadopoulos, T., Deller, T., and Betz, H. (2012). Homeostatic Regulation of Gephyrin Scaffolds and Synaptic Strength at Mature Hippocampal GABAergic Postsynapses. *Cereb Cortex*. doi:10.1093/cercor/bhs260.
- Xiang, S., Nichols, J., Rajagopalan, K.V., and Schindelin, H. (2001). The crystal structure of Escherichia coli MoeA and its relationship to the multifunctional protein gephyrin. *Structure* *9*, 299-310.
- Zita, M.M., Marchionni, I., Bottos, E., Righi, M., Del Sal, G., Cherubini, E., and Zacchi, P. (2007). Post-phosphorylation prolyl isomerisation of gephyrin represents a mechanism to modulate glycine receptors function. *Embo J* *26*, 1761-1771.

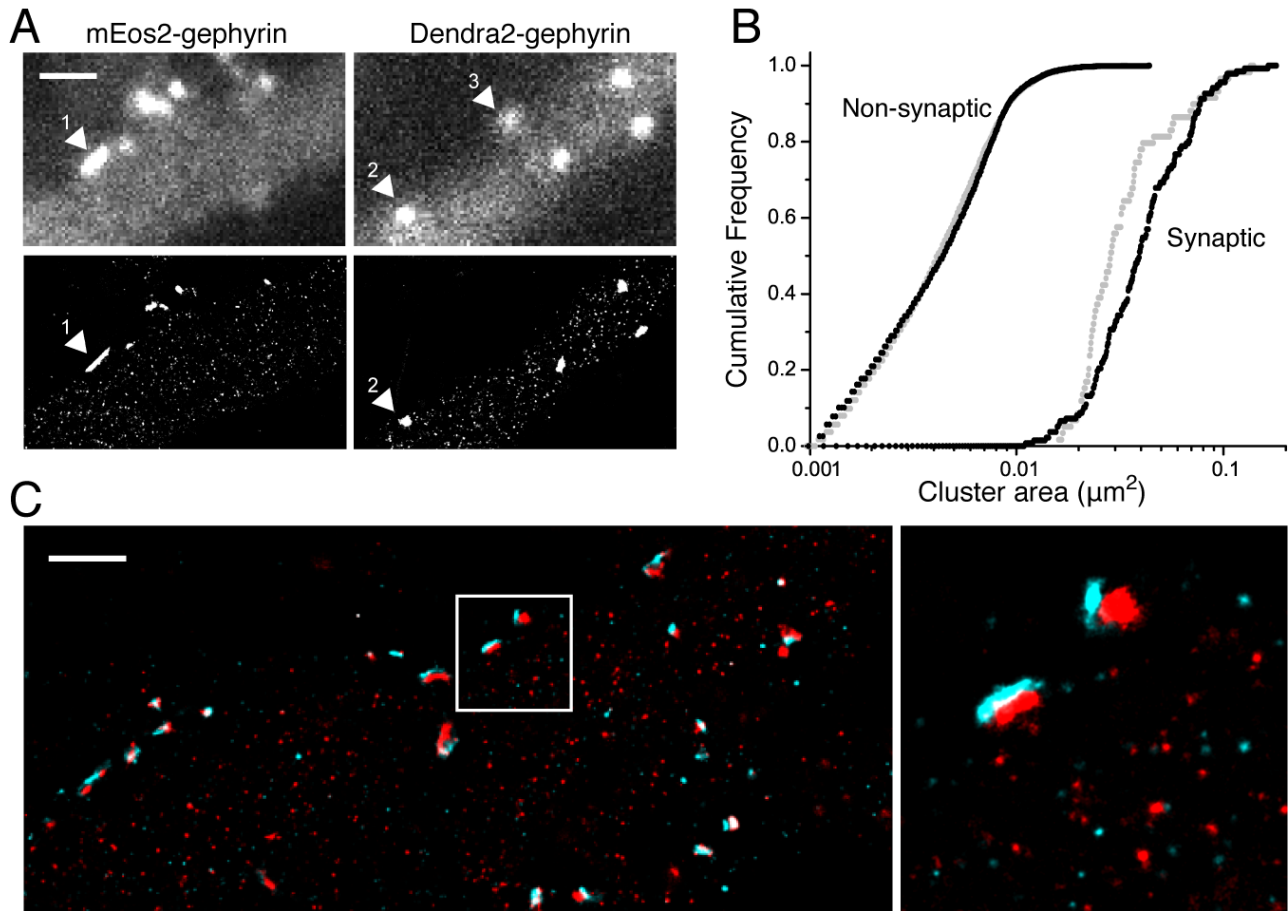
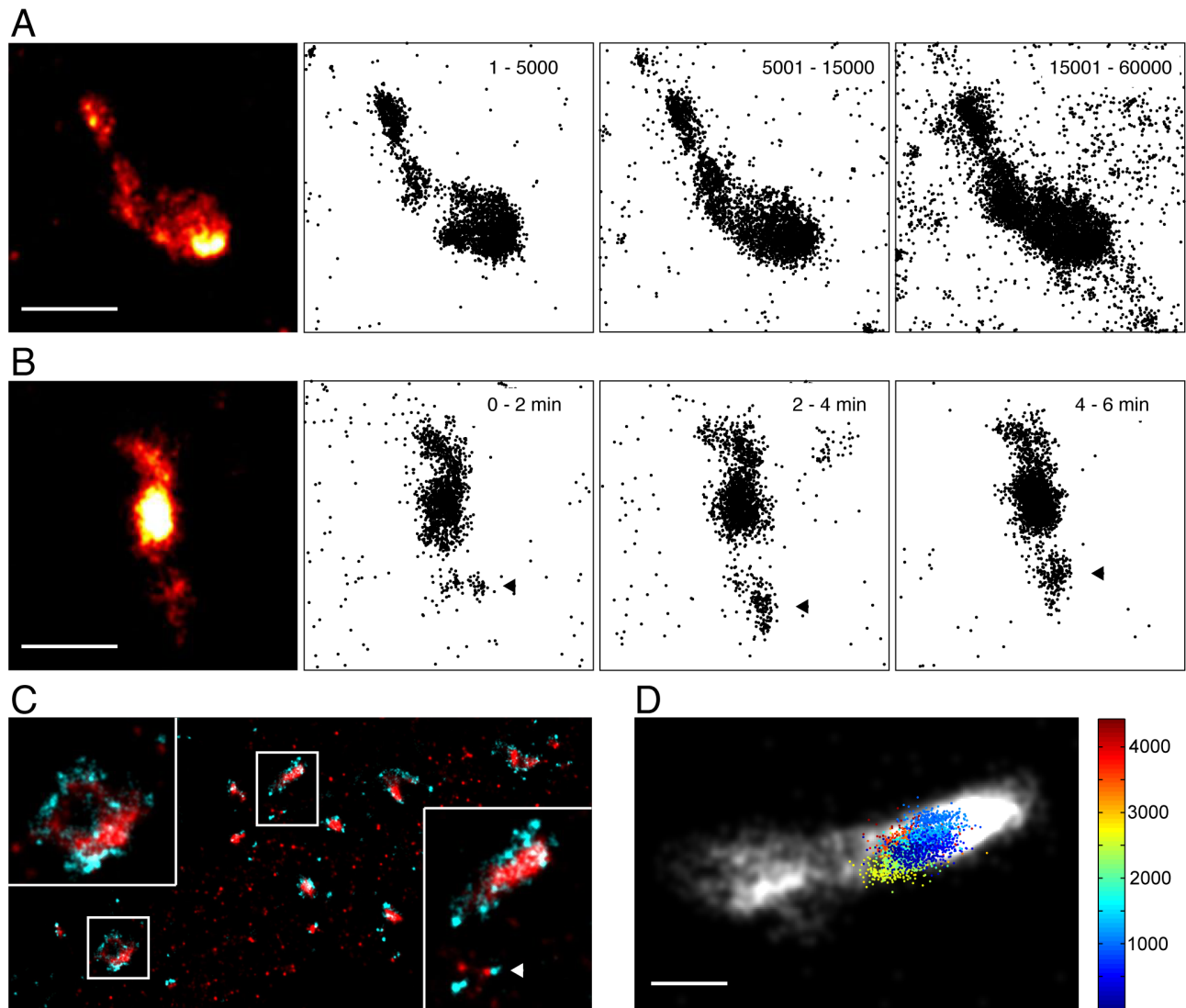


Figure 1: Single molecule imaging of gephyrin clusters at inhibitory synapses

A. PALM imaging of mEos2-gephyrin and Dendra2-gephyrin in dissociated spinal cord neurons (lower panels) distinguishes between large gephyrin clusters (arrowheads 1, 2) and a population of gephyrin nanoclusters that are not visible by conventional fluorescence microscopy (top). Note that single fluorophores are only detected close to the focal plane (e.g. cluster 3 is detected by PALM). B. Size distribution of large gephyrin clusters (synaptic) and small nanoclusters (non-synaptic). No differences were observed between mEos2-gephyrin (black) and Dendra2-gephyrin (grey) cluster sizes. C. Dual PALM/STORM imaging shows the apposition of large mEos2-gephyrin clusters (red) and Alexa 647-tagged bassoon (cyan) at synapses. Scale: 2  $\mu\text{m}$  (A, C), 3  $\mu\text{m}$  (box in C).



**Figure 2: Internal organisation of synaptic mEos2-gephyrin clusters**

A. Synaptic mEos2-gephyrin cluster in a fixed dissociated spinal cord neuron shown as a rendered reconstruction of 60000 frames (left panel, red hot) and as pointillist images of independent sets of image frames (1-5000, 5001-15000, 15001-60000) with similar total number of detections. B. Live PALM imaging of mEos2-gephyrin (20000 frames rendered image and 3 x 6000 frame pointillist images with 2 min temporal resolution). Arrowheads indicate dynamic rearrangements of a gephyrin cluster sub-domain. C. PALM/STORM of mEos2-gephyrin (red) and Alexa 647-labelled endogenous GlyR $\alpha$ 1 (cyan) in fixed spinal cord neurons shows the correspondence between the GlyR and gephyrin distributions at inhibitory synapses. Also note the co-localisation (within < 50 nm) of GlyRs and gephyrin nanoclusters (arrowhead). D. SPT-QD trajectory of a single endogenous GlyR complex (coloured pointillist projection) reveals the receptor dynamics at a mEos2-gephyrin cluster (greyscale) visualised by PALM. The colour scale indicates the frame number at 50 Hz acquisition rate (1000 frames = 20 s of recording). Scale: 500 nm (A, B); 1.25  $\mu$ m (box width in C); 200 nm (D).

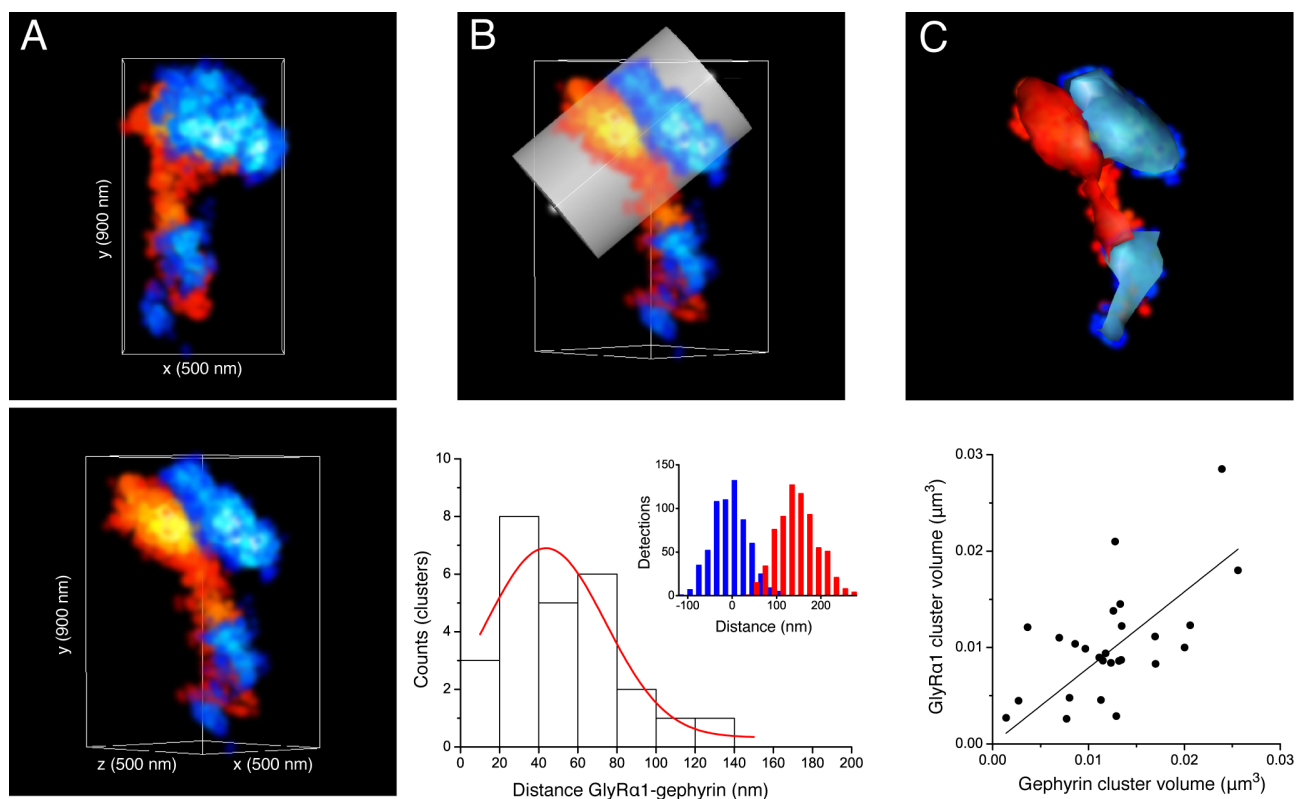


**Figure 3: 3D organisation of mEos2-gephyrin clusters at inhibitory PSDs**

A. Co-localisation of mEos2-gephyrin (red hot) and Alexa 647-tagged GlyR $\alpha$ 1 (cyan hot) in fixed spinal cord neurons, shown as x/y-view (top) and 45° perspective (bottom). The fluorophore detections are displayed in false colours according to density (number of nearest neighbours within a 50 nm sphere). B. The number of 3D-PALM/STORM detections was measured along a vertical line through the PSD with a 200 nm radius (top), to determine the width of the mEos2-gephyrin and GlyR domains (bottom). The shown cluster has an apparent width of 106 nm for gephyrin (red) and 94 nm for the GlyR domain (blue), measured as full width at half maximum (FWHM, inset). The mean distance of the GlyR and gephyrin domains along the detection profiles was  $44 \pm 6$  nm (mean  $\pm$  SEM,  $n = 26$  clusters, 13 fields of view, 3 experiments). Note that the shown example is an extreme case that was chosen for representation purposes (inset). C. Surface rendering of mEos2-gephyrin clusters (red) and GlyRs (cyan) at inhibitory synapses (overlaid with fluorophore density localisations, top image) reveals the correlation of the volumes of the two structures (slope 0.8,  $R^2 = 84$ ; bottom; see also movie S1).

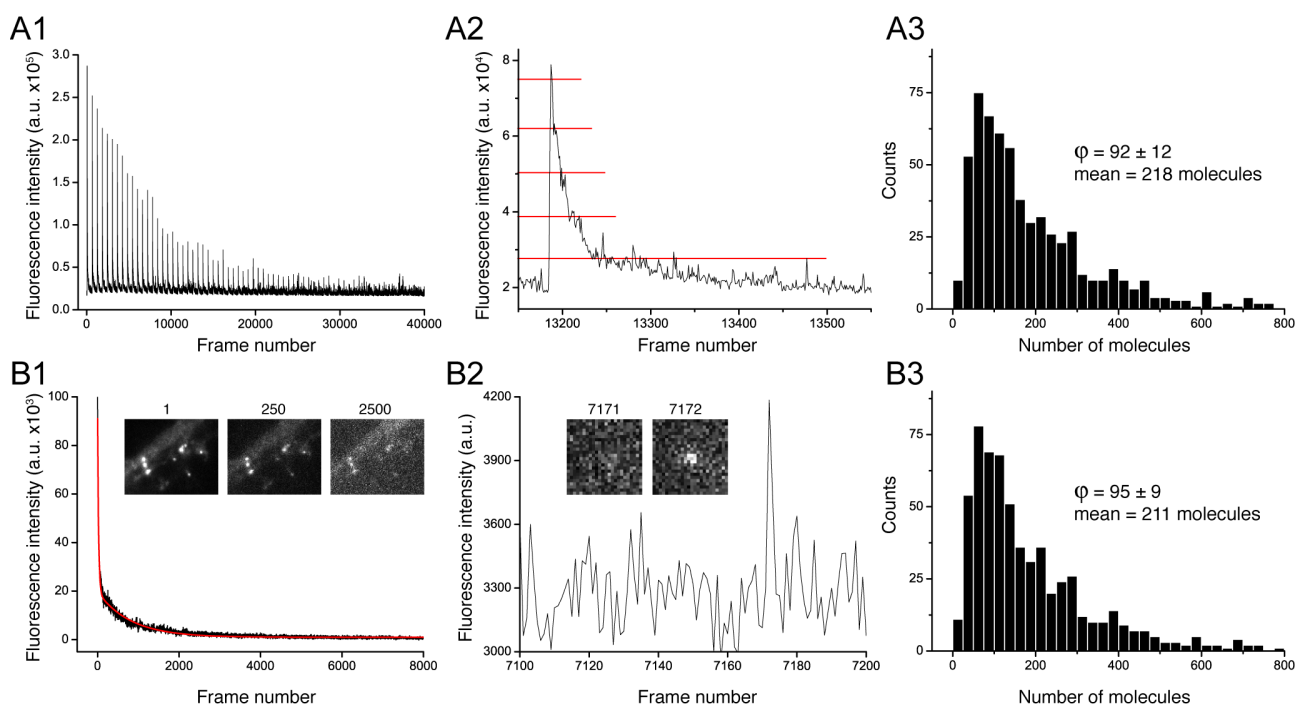


**Figure 4: Quantification of Dendra2-gephyrin molecules at synapses in fixed neurons**

A1. Pulsed photoconversion and bleaching of Dendra2-gephyrin clusters by application of trains of 100 ms pulses of 405 nm (every 30 s) during continuous illumination with 561 nm laser light. A2. The decay traces display single Dendra2 intensity steps (e.g. pulse at frame ~13200, indicated by red lines). A3. Histogram of Dendra2-gephyrin molecule numbers of synaptic gephyrin clusters in fixed dissociated spinal cord neurons, using the conversion factor  $\varphi$  obtained by pulsed photoconversion. B1. Bleaching of non-converted Dendra2-gephyrin clusters using 491 nm laser illumination (insets). The recording was fitted with a double exponential decay (red line). The extracted time constants ( $\tau_1 = 24$  frames,  $\tau_2 = 767$  frames) and amplitudes ( $a_1 = 74400$  a.u.,  $a_2 = 19000$  a.u.) were used to calculate the weighted (effective) time constant ( $\tau_w = 175$  frames in the given example). The area under the curve  $A$  represents the integrated fluorescence intensity of the cluster. B2. Blinking Dendra2-gephyrin molecules were detected at the end of the decay recordings (e.g. in frame 7172). From the distribution of these blinking events we obtained the cluster-specific mean fluorophore intensity (in the shown example  $I = 889$  a.u.). B3. Histogram of Dendra2-gephyrin molecule numbers of synaptic clusters in fixed spinal cord neurons, using the conversion factor  $\varphi$  obtained by decay recordings. Scale:  $12 \times 15 \mu\text{m}$  (B1);  $2.5 \times 2.5 \mu\text{m}$  (B2).

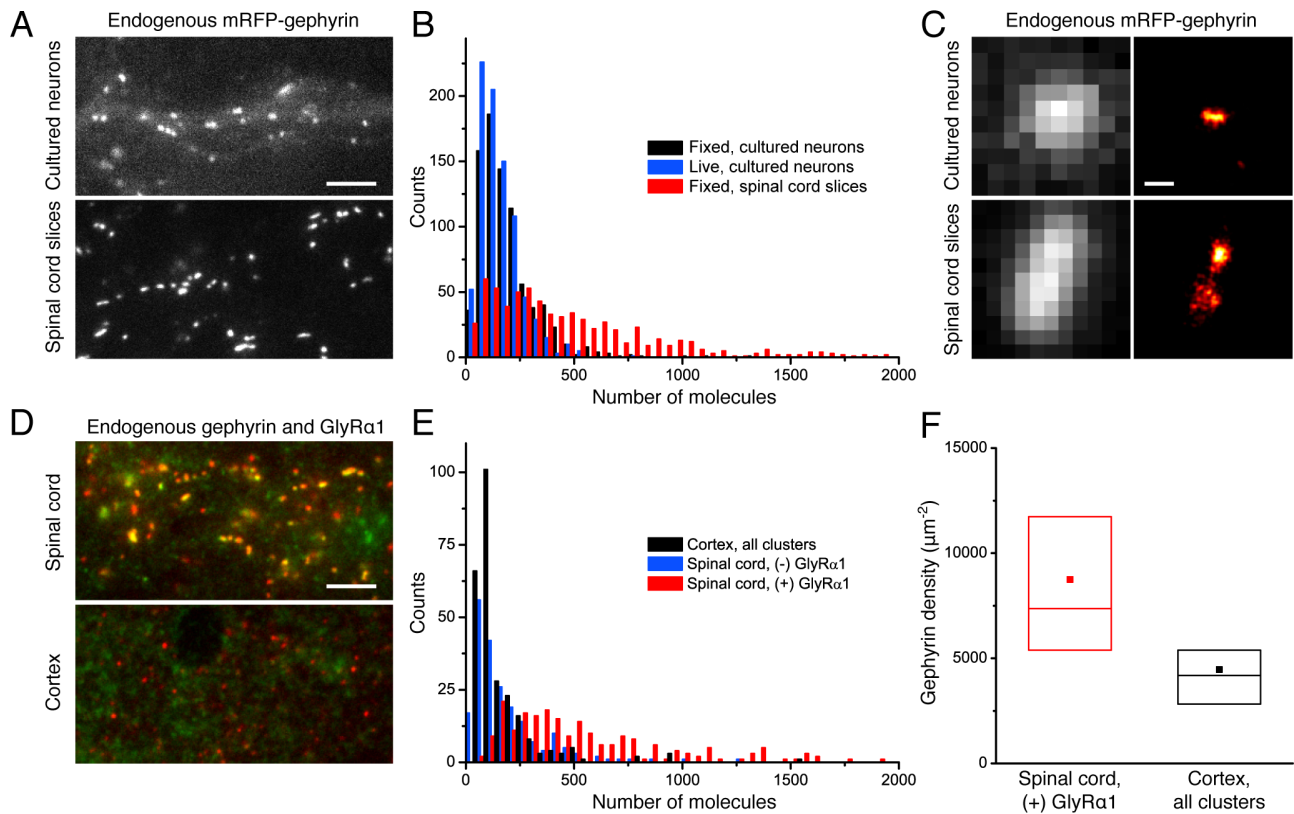


**Figure 5: Quantification of endogenous mRFP-gephyrin molecules at synapses**

A. Conventional fluorescence microscopy of endogenous mRFP-gephyrin clusters in fixed spinal cord cultures (top) and spinal cord slices (0.5  $\mu\text{m}$  thickness) from 3 month-old mRFP-gephyrin KI animals (bottom). B. Quantification of endogenous mRFP-gephyrin molecules at synapses using decay recordings in fixed (black) and living spinal cord cultures (blue), and in fixed spinal cord slices (red). C. Quantitative imaging and super-resolution image reconstruction of endogenous mRFP-gephyrin clusters was combined to calculate gephyrin densities in fixed cultures and spinal cord slices (left panels: conventional fluorescence imaging, right panels: naPALM). The shown examples have densities of 4281 molecules/ $\mu\text{m}^2$  (208 molecules, size 0.049  $\mu\text{m}^2$ , top) and 12786 molecules/ $\mu\text{m}^2$  (1514 molecules, size 0.118  $\mu\text{m}^2$ , bottom), respectively. D. Conventional imaging of endogenous mRFP-gephyrin (red) and Alexa 647-labelled GlyR $\alpha$ 1 subunits (green) in 6 month-old spinal and cortical tissue (1  $\mu\text{m}$  slices). E. Quantification of mRFP-gephyrin molecules in cortex (black) and in spinal cord inhibitory synapses that are negative (blue) or positive for endogenous GlyR $\alpha$ 1 (red). F. Distribution of gephyrin molecule densities at GlyR $\alpha$ 1-containing spinal cord synapses (red) and at cortical synapses (black), represented as box charts displaying the mean, 25%, median and 75% of the cluster population (squares, lower, middle and upper horizontal lines, respectively). Scale: 5  $\mu\text{m}$  (A,D); 200 nm (C).

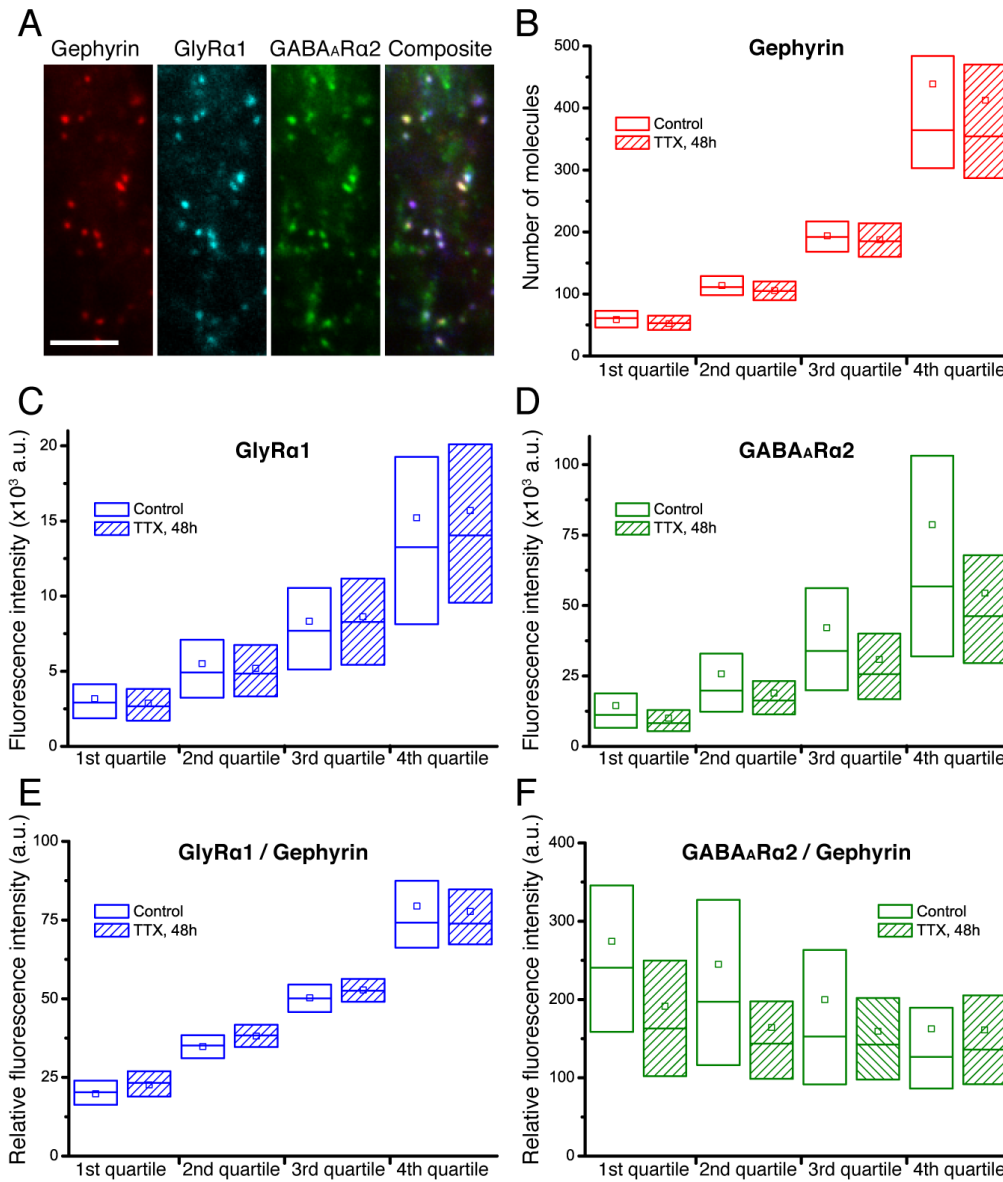


**Figure 6: Activity-dependence of GlyR and GABA<sub>A</sub>R levels at inhibitory synapses**

A. Endogenous GlyRα1 (Alexa 647, blue) and GABA<sub>A</sub>Rα2 subunits (Alexa 488, green) co-localise with endogenous mRFP-gephyrin clusters (red) in cultured spinal cord neurons. Scale: 5 μm. B-D. Synaptic clusters were binned by mRFP-gephyrin molecule number (B; 4 quartiles, each represented as box charts with mean, median, 25% and 75% of the cluster population). The largest gephyrin clusters (4<sup>th</sup> quartile) express the highest levels of GlyRs (C) and GABA<sub>A</sub>Rs (D). In cultures treated with 1 μM TTX for 48 h (hatched boxes) the GABA<sub>A</sub>Rs levels are reduced, whereas GlyRs and gephyrin numbers are unchanged ( $n_{\text{control}} = 3519$  and  $n_{\text{TTX}} = 3406$  clusters, 58 fields of view, 2 coverslips per condition). E,F. Synaptic clusters were binned by the ratio of GlyRα1 fluorescence / gephyrin number as a measure of GlyR occupancy. The clusters with the highest GlyR occupancy (4<sup>th</sup> quartile, E) express the lowest level of GABA<sub>A</sub>Rs (F). TTX treatment reduces GABA<sub>A</sub>R levels most notably in synapses with low GlyR occupancy (1<sup>st</sup> and 2<sup>nd</sup> quartiles).

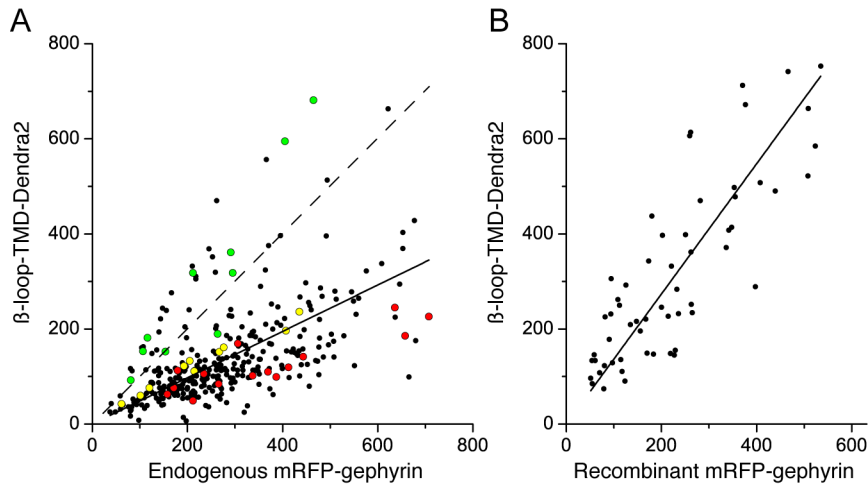


**Figure 7: Quantification of receptor binding sites at inhibitory PSDs**

A. Dual-colour quantification of the number of β-loop-TMD-Dendra2 and endogenous mRFP-gephyrin molecules in cultured spinal cord neurons (n = 347 clusters, 34 cells, 3 experiments) shows a linear relationship (slope 0.49, R<sup>2</sup> = 0.77, black line). Data points from three individual neurons with low (red), intermediate (yellow) and high (green) β-loop-TMD-Dendra2 expression are highlighted. In highly expressing cells β-loop-TMD-Dendra2 and mRFP-gephyrin are clustered close to a 1:1 ratio (dashed line). B. Quantification of β-loop-TMD-Dendra2 and recombinant mRFP-gephyrin in COS-7 cells (n = 59 clusters, 17 cells, 2 coverslips). The two proteins are clustered in a stoichiometry of 1.37:1 (black line, R<sup>2</sup> = 0.90).

**Table 1: Quantitative parameters of inhibitory synapses in cultured spinal cord neurons**

Details on how the values were obtained or calculated are given in the results section. Note that values may vary substantially in mature synapses *in vivo* or in response to synaptic plasticity. Given the limited spatial resolution of 3D-PALM, the thickness and volume readings are upper limits.

	mean (range)	notes
size of inhibitory PSD	0.05 (0.01-0.1) μm <sup>2</sup>	2D projection
thickness of gephyrin scaffold	≤ 100 nm	3D measurement
volume of gephyrin scaffold	≤ 0.012 μm <sup>3</sup>	3D measurement
distance gephyrin – synaptic cleft	44 nm	3D measurement
number of endogenous mRFP-gephyrin molecules	200 (40-500) molecules / cluster	<i>in vivo</i> : cortical synapses (adult): 130 molecules / cluster spinal cord (adult, GlyRα1 positive): 600 / cluster
surface density of gephyrin clusters	5000 gephyrin molecules / μm <sup>2</sup>	<i>in vivo</i> : cortical synapses (adult): 4500 molecules / μm <sup>2</sup> spinal cord (adult, GlyRα1 positive): 9000 / μm <sup>2</sup>
number of GlyRβ binding sites	1 binding site / gephyrin molecule	receptor occupancy ≤ 1